2nd AIAA Flow Control Conference, June 28 – July 1, 2004, Portland, OR, USA

Low-Dimensional Models For Feedback Flow Control. Part II: Control Design and Dynamic Estimation*

Gilead Tadmor†
Northeastern University, 440 Dana Research Building, Boston, MA 02115, U.S.A.

Bernd R. Noack‡
Technical University of Berlin HF1, Straße des 17. Juni, 10623 Berlin, Germany

Marek Morzyński§
Poznan University of Technology, Piotrowo 3, 60-965 Poznan, Poland

Stefan Siegel ¶
US Air Force Academy, CO 80840, U.S.A, AIAA member

Control design and dynamic estimation are developed for a feedback flow control strategy based on very low order empirical Galerkin models developed in Part I (AIAA Paper 2004-2408). The suppression of vortex shedding behind an oscillating cylinder is used as a benchmark problem. A systematic DNS investigation of the controlled wake corroborates predictions of the corresponding 4-dimensional Galerkin model. The model's predictive power is improved by dynamic estimation.

Nomenclature

$\mathbf{x}$	Location
$x_{\rm rec}$	Length of the recirculation zone
$y_{\rm cyl}$	Transverse position of the cylinder
t	Time
$\mathbf{u}$	Velocity field
$\mathbf{u}_s$	Steady Navier-Stokes solution
$\mathbf{u}_i$	i-th expansion mode of the Galerkin approximation
$\mathbf{u}_c$	Actuation mode associated with transverse cylinder oscillation
a_i	Fourier coefficient of the i-th expansion mode
a_c	Amplitude of the actuation mode
ϕ	Phase of the transverse oscillation
A	Amplitude of the transverse cylinder oscillation
$\alpha, \beta, \gamma, \sigma_r, \sigma_3, \omega$	Galerkin system coefficients describing the natural dynamics
r, θ	Polar coordinate representation of a_1,a_2
θ_c	Phase difference between actuation and flow phase
θ_{ol}	Phase difference between actuation and flow phase under open-loop actuation

*This paper was invited by the AIAA Architecture and Algorithms Working Group headed by Prof. David Williams and Dr. Andrzej Banaszuk

†Professor, Communication & Digital Signal Processing Center, Department of Electrical and Computer Engineering, AIAA member

‡Research Engineer, Hermann-Föttinger-Institute of Fluid Mechanics, AIAA member

§Professor, Institute of Combustion Engines and Basics of Machine Design

¶Assistant Research Professor, Department of Aeronautics, AIAA member

$\Delta\phi$	Phase offset under closed-loop control
Γ	Amplitude of the ficticious volume force
g_1, g_2	Galerkin system coefficients associated with the volume force
$\kappa_i, \kappa_{i,j}$	Galerkin system coefficients associated with the cylinder oscillation
g_r, g_θ, g_3	forcing terms of the Galerkin system in cylindrical coordinates
'$\_$'	Denotes a one-period average
$\langle \quad \rangle$	Denotes the time average
Other quantities	relate to parameter estimation in the appendix

I. Introduction

In the current study, the suppression of laminar vortex shedding behind a transversely oscillating circular cylinder is used as a testbed for a feedback flow control strategy based on low-dimensional empirical Galerkin models.[1] The suppression of the von Kármán vortex street has been a benchmark problem for many flow control strategies. Significant reductions of the wake oscillations have been achieved with passive means, like splitter plates,[2,3,4] control cylinders[5] and with open-loop actuation, like base bleeding[6] and oscillatory cylinder rotation.[7]

Model-based feedback flow control stabilizations of the nearly steady wake have been performed with a large variety of models. Examples of numerically or experimentally validated controllers are

1. a black-box control using loudspeakers,[8]
2. an optimal control employing oscillatory cylinder rotation,[9]
3. an optimal control based on continually updated empirical Galerkin models using a local volume force,[10]
4. an optimal control based on a higher-dimensional empirical Galerkin model using a cylinder rotation,[11]
5. a flatness-based control from a low-dimensional vortex model applying cylinder rotation,[12]
6. an energy-based control derived from a Galerkin model with a volume force actuator,[13] and
7. a PD control from the first Karhunen-Loève coefficient using transverse cylinder oscillations.[14]

In the current study, an opposition control strategy for transverse cylinder oscillation is developed based on work of the USAFA team[14] (see Fig. 1). This strategy leads to robust energy-based control employing a least-order Galerkin model. The manuscript is organized as follows. First (§II), a minimal Galerkin model is derived from the recipes of Part I.[1] For that model, a corresponding controller is designed in §III. In §IV, Navier-Stokes simulations are presented for a controlled cylinder wake. The conclusions are summarized in §V. A dynamic estimation technique for parameter calibration of the least-order Galerkin model is presented in §A

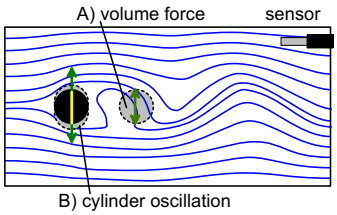

Figure 1. Principal sketch of the cylinder wake with actuation and sensor. Two kinds of actuations have been investigated: (A) a local volume force,[13] and (B) transverse cylinder oscillation (current study).

II. Galerkin model with actuation

In this section, a least-order model is distilled from the Galerkin modelling toolbox of Part I.[1] First (§A), a minimal representation of the natural dynamics is reviewed. The incorporation of a volume force and cylinder motion as actuators are described in §B and §C, respectively.

A. Minimal Galerkin model for the natural flow

The starting point of the model development is a Galerkin approximation based on the (unstable) steady Navier-Stokes solution $\mathbf{u}_s$, the first two Karhunen-Loève modes $\mathbf{u}_{1,2}$ and the shift mode as the third mode

$\mathbf{u}_3$,

$$\mathbf{u} = \mathbf{u}_s + a_1\mathbf{u}_1 + a_2\mathbf{u}_2 + a_3\mathbf{u}_3. \tag{1}$$

This ansatz neglects about 5% of the fluctuation energy of the limit cycle and is equivalent to Eq. (3) of Ref. 1 with an offset in the shift-mode amplitude a_3.

The corresponding Galerkin system (5) of Part I can be phase-averaged without noticeable loss of accuracy.[15] This procedure yields the dynamical system

$$\frac{d}{dt}\begin{bmatrix} a_1 \\ a_2 \\ a_3 \end{bmatrix} = \begin{bmatrix} \sigma_r & -\omega-\gamma a_3 & -\beta a_1 \\ \omega+\gamma a_3 & \sigma_r & -\beta a_2 \\ \alpha a_1 & \alpha a_2 & -\sigma_3 \end{bmatrix} \begin{bmatrix} a_1 \\ a_2 \\ a_3 \end{bmatrix} \tag{2}$$

with only 6 model parameters $(\alpha, \beta, \gamma, \sigma_0, \sigma_3, \omega)$ as opposed to 60 of the original system. Here, $\sigma_0, \beta > 0$ guarantee the existence of a globally stable limit cycle.

A transformation to cylindrical coordinates r, θ, a_3 via

$$a_1 = r\,\cos(\theta), \qquad a_2 = r\,\sin(\theta) \tag{3}$$

yields

$$\frac{d}{dt}\begin{bmatrix} r \\ a_3 \end{bmatrix} = \begin{bmatrix} \sigma_r & -\beta r \\ \alpha r & -\sigma_3 \end{bmatrix} \begin{bmatrix} r \\ a_3 \end{bmatrix}, \qquad \frac{d}{dt}\theta = \omega + \gamma a_3. \tag{4}$$

with the stable limit cycle

$$a_{3*} = \frac{\sigma_r}{\beta}, \qquad r_* = \sqrt{\frac{\sigma_3}{\alpha}a_{3*}} = \sqrt{\frac{\sigma_3\sigma_r}{\alpha\beta}}. \tag{5}$$

B. Incorporation of the volume force

The oscillating cylinder is described in a body-fixed coordinate system (see §VII of Part I). Hence, a ficticious transverse volume force representation has to be added to Eqn. (2) accounting for the cylinder acceleration,

$$\frac{d}{dt}\begin{bmatrix} a_1 \\ a_2 \\ a_3 \end{bmatrix} = \begin{bmatrix} \sigma_r & -\omega-\gamma a_3 & -\beta a_1 \\ \omega+\gamma a_3 & \sigma_r & -\beta a_2 \\ \alpha a_1 & \alpha a_2 & -\sigma_3 \end{bmatrix} \begin{bmatrix} a_1 \\ a_2 \\ a_3 \end{bmatrix} + \begin{bmatrix} g_1 \\ g_2 \\ 0 \end{bmatrix} \Gamma. \tag{6}$$

with the new coefficients g_1, g_2 and $\Gamma = -\ddot{y}_{\mathrm{cyl}} = \dot{a}_c$. Note that the dynamics of the shift mode is not directly affected by the volume force due to reasons of symmetry.

C. Incorporation of the cylinder oscillation

The free-stream oscillation requires an actuation mode contribution $a_c\mathbf{u}_c$ to the Galerkin ansatz (1) as described in Part I. The resulting Galerkin system is expressed by

$$\frac{d}{dt}\begin{bmatrix} a_1 \\ a_2 \\ a_3 \\ a_c \end{bmatrix} = \begin{bmatrix} \sigma_r & \omega+\gamma a_3 & -\beta a_1 & \kappa_1+\kappa_{1,3}a_3 \\ -\omega-\gamma a_3 & \sigma_r & -\beta a_2 & \kappa_2+\kappa_{2,3}a_3 \\ \alpha a_1 & \alpha a_2 & -\sigma_3 & \kappa_3+\kappa_{3,1}a_1+\kappa_{3,2}a_2+\kappa_{3,c}a_c \\ 0 & 0 & 0 & 0 \end{bmatrix} \begin{bmatrix} a_1 \\ a_2 \\ a_3 \\ a_c \end{bmatrix} + \begin{bmatrix} b_1 \\ b_2 \\ 0 \\ 1 \end{bmatrix} \Gamma. \tag{7}$$

The coefficients κ_i, κ_{ij} describe the coupling of the flow dynamics with the control input a_c and can easily be determined from the Galerkin system coefficients l_{ij}, q_{ijk} in Eqn. (7) of Part I. The fourth equation implies $\Gamma = da_c/dt$ as derived in Part I.

A transformation into cylindrical coordinates (3) yields additional forcing terms in Eqn. (4),

$$\begin{aligned} \tfrac{d}{dt}\begin{bmatrix} r \\ a_3 \end{bmatrix} &= \begin{bmatrix} \sigma_r & -\beta r \\ \alpha r & -\sigma_3 \end{bmatrix} \begin{bmatrix} r \\ a_3 \end{bmatrix} + \begin{bmatrix} g_r(\theta, a_3, a_c, \dot{a}_c) \\ g_3(a, a_c) \end{bmatrix} \\ \tfrac{d}{dt}\theta &= \omega + \gamma a_3 + g_\theta(\theta, a_3, a_c, \dot{a}_c) \end{aligned} \tag{8}$$

where

$$\begin{aligned} g_r(\theta, a, a_c, \dot{a}_c) &= \cos(\theta)\ [(\kappa_1 + \kappa_{1,3} a_3) a_c + b_1 \dot{a}_c] + \sin(\theta)\ [(\kappa_2 + \kappa_{2,3} a_3) a_c + b_2 \dot{a}_c]\,, \\ g_\theta(\theta, a, a_c, \dot{a}_c) &= \frac{1}{r}\left\{\cos(\theta)\ [(\kappa_2 + \kappa_{2,3} a_3) a_c + b_2 \dot{a}_c] - \sin(\theta)\ [(\kappa_1 + \kappa_{1,3} a_3) a_c + b_1 \dot{a}_c]\right\}, \\ g_3(a, a_c) &= (\kappa_{3,1} a_1 + \kappa_{3,2} a_2 + \kappa_{3,c} a_c)\ a_c. \end{aligned}$$

We assume a slowly varying oscillatory control input of the form

$$a_c = r_c\ \cos(\phi) = r_c\ \cos(\theta - \theta_c), \quad \frac{d}{dt} a_c \approx -\dot{\phi} r_c\ \sin(\phi) \approx -(\omega + \gamma\, a_3)\, r_c\ \sin(\theta - \theta_c) \tag{9}$$

where r_c represents the velocity amplitude, ϕ the phase of the control, and θ_c the phase difference between control and flow.

A one-period average of ansatz (9) in (8) yields following dc components of the forcing term:

$$\overline{g}_r \approx 0.5 r_c \left\{\cos(\theta_c)\ [\kappa_1 + \kappa_{1\,3} a_3 - b_2(\omega + \gamma a_3)] + \sin(\theta_c)\ [\kappa_2 + \kappa_{2\,3} a_3 + b_1(\omega + \gamma a_3)]\right\} \tag{10}$$

$$\overline{g}_\theta \approx 0.5 r_c \left\{\cos(\theta_c)\ [\kappa_2 + \kappa_{2\,3} a_3 + b_1(\omega + \gamma a_3)] - \sin(\theta_c)\ [\kappa_1 + \kappa_{1\,3} a_3 - b_2(\omega + \gamma a_3)]\right\} \tag{11}$$

$$\overline{g}_3 \approx 0.5 r_c \left\{[\kappa_{3\,1} \cos(\theta_c) + \kappa_{3\,2} \sin(\theta_c)]\, r + \kappa_{3\,c} r_c\right\}. \tag{12}$$

The largest amplitude decay r at a given forcing amplitude r_c is obtained when θ_c is chosen according to

$$\begin{bmatrix} \cos(\theta_c) \\ \sin(\theta_c) \end{bmatrix} \propto \begin{bmatrix} \kappa_1 + \kappa_{1\,3} a_3 - b_2(\omega + \gamma a_3) \\ \kappa_2 + \kappa_{2\,3} a_3 + b_1(\omega + \gamma a_3) \end{bmatrix} \perp \begin{bmatrix} \kappa_2 + \kappa_{2\,3} a_3 + b_1(\omega + \gamma a_3) \\ -(\kappa_1 + \kappa_{1\,3} a_3 - b_2(\omega + \gamma a_3)) \end{bmatrix}. \tag{13}$$

The $\perp$ sign indicates that the most energy efficient θ_c for amplitude reduction (or enhancement) coincides with a vanishing effect of the control on the frequency. The control amplitude r_c can be determined from a prescribed exponential decay of the fluctuation amplitude r, as elaborated in Ref. 16.

III. Control design based on the Galerkin model

The Galerkin system (8) is employed for a heuristic analysis of the actuation effect on the flow dynamics. The corresponding amplitude equation is expressed by

$$\frac{d}{dt} r = (\sigma_r - \beta\, a_3)\ r + g. \tag{14}$$

In addition, the inertial manifold relation of natural dynamics is exploited,[15]

$$a_3 = (\alpha/\sigma_3)\, r^2. \tag{15}$$

For reasons of simplicity, g is assumed constant. The implications of the Galerkin model can be read from Eqs. (14,15) and have been numerically validated:

1. The natural flow has an unstable steady solution at the origin $r = a_3 = 0$ corresponding to $\mathbf{u}_s$ in Eqn. (1).

2. The natural flow has a globally stable limit cycle described by Eqn. (5).

3. Open-loop forcing tends to increase the energy level by choosing a phase $\theta_c = \theta_{ol}$ which nearly optimizes the energy extraction of the mean flow. In terms of the amplitude equation (14), this implies $g < 0$ and an increase of a_Δ (see Fig. 1).

4. Closed-loop forcing with constant amplitude r_c and constant phase θ_c can reduce the oscillation amplitude r. There exists a single stable limit cycle (see Fig. 1).

5. Moreover, there exist another limit cycle with lower energy, if the amplitude is not too large. This limit cycle can be shown to be unstable from Eqn. (14), i.e. cannot be realized as steady state under our control policy.

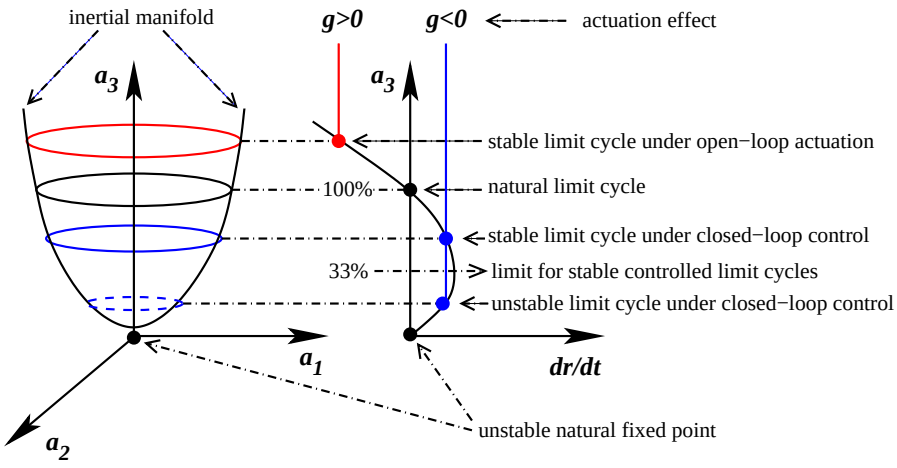

Figure 2. Principal sketch of the solutions associated with Eqn. (14).

6. The largest achievable reduction is 2/3 of the natural fluctuation energy — assuming again a feedback control policy with the constant amplitude r_c and constant phase.

7. A stabilization of the unstable steady solution requires a different feedback control law where g vanishes as $r \to 0$.

All these statements are also numerically corroborated in our flow simulations.

In the current study, we adopt a simple control strategy motivated by this analysis,

$$a_c = A\ \cos(\theta - \theta_c), \quad A = \text{constant}, \quad \theta_c = \text{constant}. \tag{16}$$

The minimal Galerkin model is quantitatively validated near the open-loop limit cycle,[16] but the coefficients quickly change as control suppresses vortex shedding. In particular, the dominant κ_i coefficients are found to be strongly dependent on the base flow. In contrast, the validity range of Galerkin model based on a local volume force is observed to be significantly larger.[13]

IV. Feedback flow control of the cylinder wake

Open- and closed-loop control is applied to the cylinder motion at $Re = 100$. The open-loop actuation is given by

$$a_c = -\dot{y}_{\text{cyl}} = A\ \cos\omega t = A\cos(\theta - \theta_{ol}), \tag{17}$$

where ω is the natural shedding frequency and the second equality expresses a definition for open-loop phase difference between flow phase and actuation. The closed-loop control imposes a phase difference $\Delta\phi$ with respect to the open-loop forcing,

$$a_c = A\cos(\phi), \quad \phi = \theta - \theta_c, \quad \theta_c = \theta_{ol} - \Delta\phi. \tag{18}$$

The flow phase is measured with respect to Karhunen-Loève modes of open-loop forcing in the near wake of the computational domain ($x \leq 6$). This domain size has been chosen to compare our results with a similar study of the USAFA team.[14] The open-loop actuation amplitude for the reference simulation is $A = 0.06$.

Figure 3 visualizes the natural flow as well as the wake under open-loop and closed-loop forcing. Open-loop actuation reduces the recirculation region whereupon closed-loop control re-laminarizes the near wake. For closed-loop control (18), the optimal phase difference $\Delta\phi = 210°$ of Siegel, Cohen and McLaughlin[14] has been adopted. It may be noted that significantly longer recirculation regions are achievable with Karhunen-Loève modes based on shorter observation regions, e.g. $x \leq 4\,D$.

Figure 4 displays a transient from open-loop forcing to closed-loop control via the natural state. The fluctuation amplitude decreases during this transient and the shift-mode amplitude gets closer to the fixed

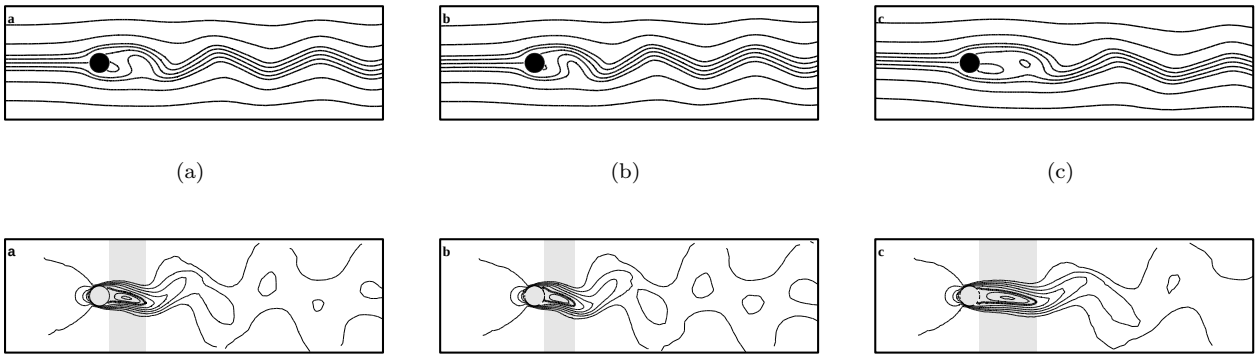

Figure 3. Snapshots of the natural (a,d), open-loop actuated (b,e) and closed-loop controlled wake (c,f). Actuation is provided by a transversely oscillating cylinder. The amplitude of open-loop actuation is $A = 0.06$. Closed-loop control is employed at the amplitude $A = 0.03$ and at the phase difference $\Delta\phi = 210°$. The cylinder is indicated by a solid disk. In the top row (a-c), the snapshots are visualized by streamlines, in the bottom row (d-f), iso-lines of the u velocity component are shown for the same snapshots. The corresponding levels are $u = -0.2$, -0.1, 0, 0.2, 0.4, 0.6, 0.8 and 1.0. The shaded rectangle illustrates the streamwise extension of the instantaneous recirculation region.

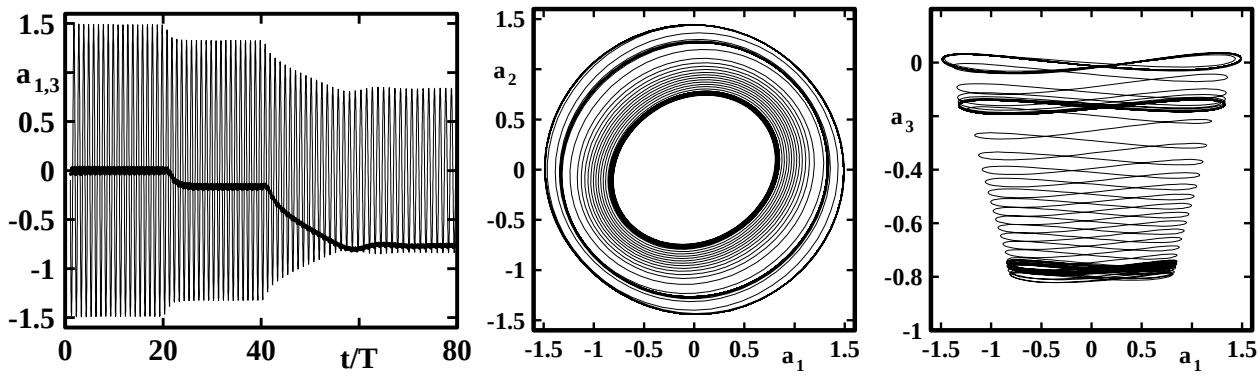

Figure 4. Transient from open-loop actuated flow ($t < 20\,T$) to closed-loop controlled flow ($t > 40\,T$) via the natural condition as intermediate state. The parameters are the same as in Fig. 3. The Fourier coefficients a_1 (thin curve) and a_3 (thick curve) are shown as a function of time t normalized with the natural shedding period T (figure *a*). Figures *b,c* display phase portraits of the first three Fourier coefficients a_1, a_2, a_3.

point value $a_3 = -2.2$.[a] As expected from Fig. 1, the trajectory $t \mapsto a_1, a_2, a_3$ spirals downward close to the inertial manifold paraboloid. The relative reduction of the oscillation amplitude in a_1 is about 50% and compares well with the reduction achieved in the study of the USAFA team.[14]

Intriguingly, chirp excitations may also drive the flow to a weakly unstable limit cycle, the existence of which has been predicted by the Galerkin model. Figure 5 shows a transient from an unstable to a stable limit cycle. The actuation and phase difference are keep constant during this 50 period long transient.

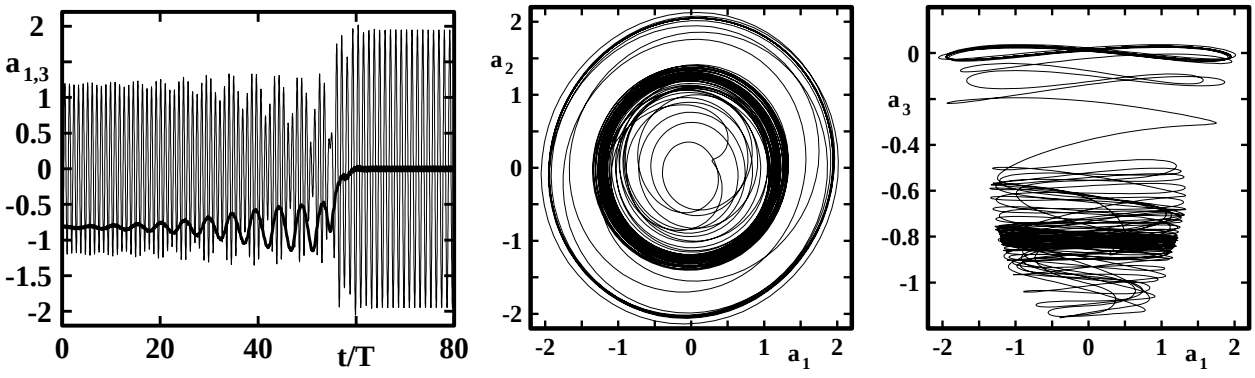

(a) (b) (c)

Figure 5. Same as Fig. 4, but for the transient from an unstable to the stable limit cycle under closed-loop control. The parameters of actuation are $A = 0.10$ and $\Delta\phi = 270°$ throughout the transient. The Karhunen-Loève decomposition is carried out in a larger domain $x \leq 10$. For smaller observation regions, the transient phases are shorter.

A parametric amplitude variation yields $A_{\text{opt}} \approx 0.03$ for the smallest fluctuation energy TKE in the near-wake $x \leq 6$ (see Fig. 6). This minimum coincides well with the minimum of the energy resolved by the two Karhunen-Loève modes, i.e. $\langle a_1^2 + a_2^2 \rangle / 2$. Note that the Karhunen-Loève modes resolve less than 50% at $A = 0.1$, i.e. other modes are excited at large amplitudes. This analysis corroborates the identification of an optimal actuation amplitude in Ref. 14. The minimum fluctuation energy of Fig. 6*a* coincides well

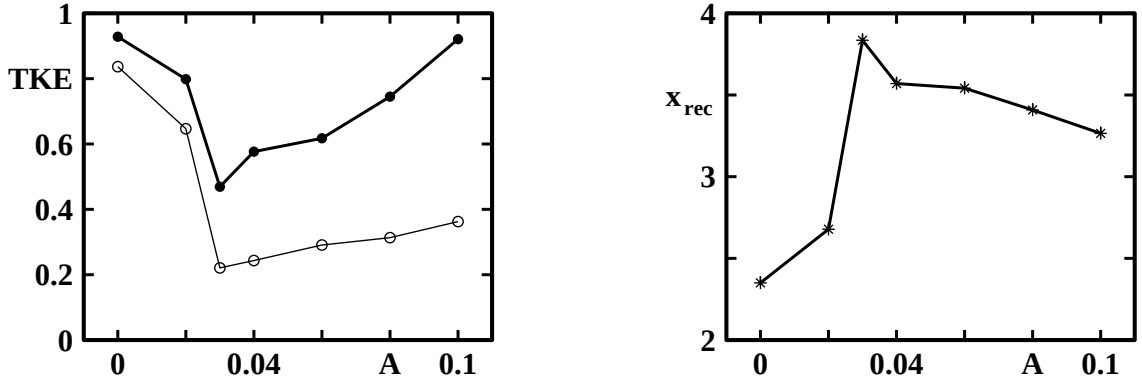

(a) (b)

Figure 6. Control measures under closed-loop actuation. The figure displays the averaged fluctuation energy K (•, figure *a*), the averaged resolved fluctuation energy $\langle a_1^2 + a_2^2 \rangle / 2$ (∘, figure *a*), and the averaged recirculation length x_{rec} (⋆, figure *b*) in dependency of the actuation amplitude A. The phase difference between open and closed-loop forcing is $\Delta\phi = 210°$.

with the maximum near-wake re-laminarization quantified by the recirculation bubble length x_{rec}. We adopt

[a] In this section, the $a_3 = 0$ corresponds to the limit cycle, i.e. the notation of Part I is adopted.

this length as our control measure since it is physically appealing and since it has the advantage of being independent of the observation region.

A systematic variation of the actuation amplitude $A \leq 0.1$ and phase difference $\Delta\phi \in [0°, 360°]$ strongly suggests that the closed-loop actuation always gives rise to a unique stable periodic limit cycle independent of the initial condition. This observation is consistent with the prediction of a globally stable limit of the Galerkin model under open- and closed-loop actuation. The transient time may be as large as 50 periods (see Fig. 5, for instance) and may be reduced by a state-space dependent phase variation.[14,16] From Fig. 7, the optimal parameters for vortex shedding suppression can be identified: $A_{\text{opt}} = 0.03$ and

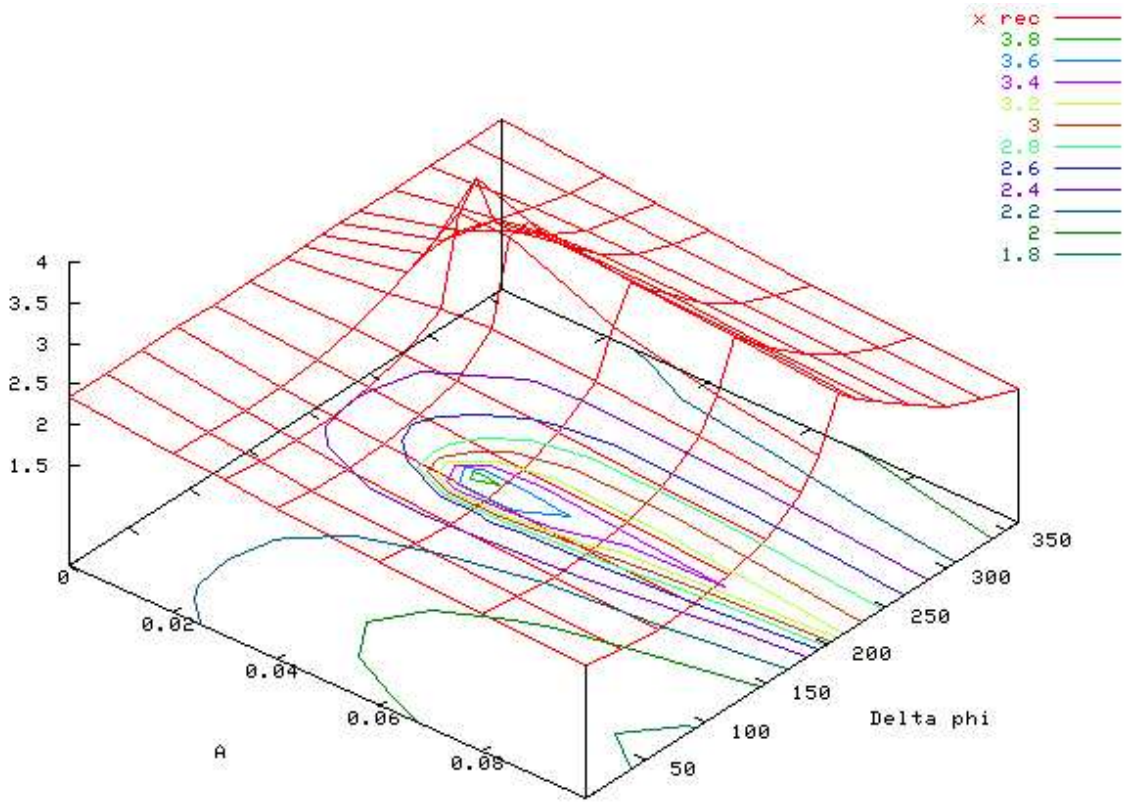

Figure 7. Recirculation length x_{rec} of the closed-loop actuated cylinder wake as a function of the amplitude A and phase difference $\Delta\phi$.

$\Delta\phi_{\text{opt}} = 210°$. Intriguingly, the shortest recirculation zone is not obtained under open-loop control ($\Delta\phi = 0$) but at ($\Delta\phi_{\text{max}} \approx 40°$). Similarly, the optimal re-laminarization is not achieved at $\Delta\phi = 180°$ — as the opposition control idea may suggest — but at $\Delta\phi_{\text{opt}} \approx 210°$. Yet, the most amplified and most suppressed closed-loop vortex shedding states are almost 180 degrees apart. This 180 degree difference is also predicted by the Galerkin model.

V. Conclusions

A 4-dimensional Galerkin model is proposed for the vortex shedding behind a circular cylinder with oscillatory transverse motion. An energy-based control design based on that model yields an opposition-type control law, which we adopt in a simplified manner for Navier-Stokes simulations. The model has a very narrow region of validity, since the accuracy of the underlying Karhunen-Loève decomposition rapidly deteriorates under a change of actuation. However, the model qualitatively explains all numerical simulation results in remarkable details. Examples include the existence of a globally stable and unstable limit cycle under closed-loop control besides the existence of a lower bound for the achievable fluctuation energy under our feedback control policy. In §A, a model estimation path is discussed for the calibration of that reduced-order model.

A. Model parameter estimation

In Part I, we discussed pressure and turbulence models as means to compensate energy dynamics that are neglected in a standard Galerkin projection, leading to distorted predictions by the Galerkin system. The over-predicted limit cycle amplitude in the reduced-order wake model is an example. Yet another cause for mismatch include the fact that an empirical Galerkin model of an attractor may not be capable to predict dynamic properties at another operating point. As shown in Noack et al.,[15] good prediction may be achieved by a sufficiently enriched model: In the cylinder wake this includes an 11-mode model, comprising four attractor harmonics, a shift mode and two leading stability analysis modes. Our goal here is to illustrate the advantages of an alternative (or complementary) approach by which parameter estimation methods are applied to achieve a posteriori correction of the distortions in a very low order model. Our simple benchmark example — the unactuated three state cylinder wake model — provides a compelling illustration (Fig. 8).

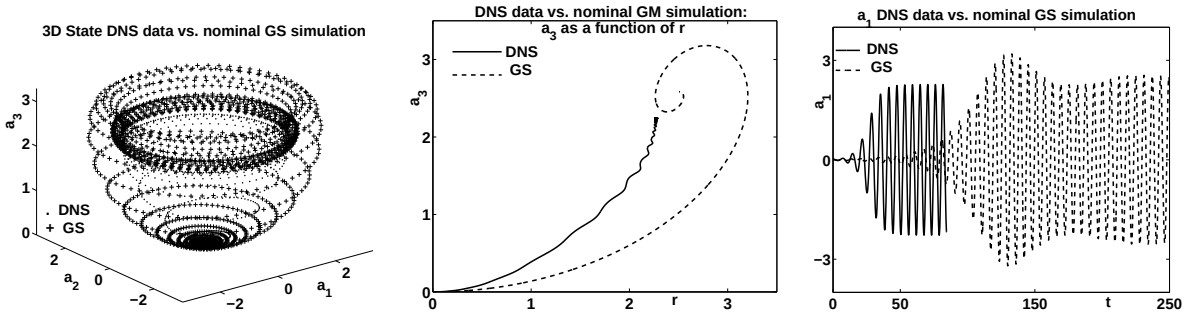

Figure 8. DNS data and a nominal Galerkin system simulations, depicting the invariant manifold formed by transients from the unstable steady solution to the attractor. Left: dynamics of of the three leading Fourier coefficients. Middle: a crosscut of the invariant manifold, showing the shift mode a_3 as a function of the oscillation amplitude r. Right: The time trajectory of a_1.

Estimation of the parameters α, β, γ, σ_r, σ_3, and ω is based on DNS data of time trajectories of the Fourier coefficients.

The estimation task falls into the general form of a Galerkin system, written in the form

$$\frac{d}{dt}\mathbf{a} = F(\mathbf{a})\sigma + G(\mathbf{a}) \tag{19}$$

where $\mathbf{a}$ is the vector of Fourier coefficients, $\sigma := [\sigma_1, \ldots, \sigma_\theta]^T$ comprises the unknown parameters, and $F(\mathbf{a})$ and $G(\mathbf{a})$ are, respectively, a quadratic matrix- and vector-valued polynomials in the entries of $\mathbf{a}$. The two approaches reviewed here adhere to the observation (see e.g., Ljung[17]) that — in contrast to the rich theory for the linear case — the identification of a nonlinear model for a system often reduces to a question of curve fitting rather than modelling. We then illustrate the application of these procedures in the context of (8).

A. Dissipative Dynamic Estimation

An appeal to dynamic dissipation is common in estimation, adaptation and control design.[18,19,20] The dynamic dissipative estimator is of the form

$$\frac{d}{dt}\widehat{\mathbf{a}} = -d\{\delta\}\triangle\mathbf{a} + F(\mathbf{a})\widehat{\sigma} + G(\mathbf{a}) \tag{20a}$$

$$\frac{d}{dt}\widehat{\sigma} = -F\{\mathbf{a}\}^T\, d\{\alpha\}^2\, \triangle\mathbf{a}, \tag{20b}$$

where, as usual, a hat "$\widehat{\ }$" indicates an estimate and "$\triangle$", the estimation error (i.e., $\triangle\mathbf{a} = \mathbf{a} - \widehat{\mathbf{a}}$), $\alpha = [\alpha_1, , \alpha_2 \ldots\ ]^T$ and $\delta = [\delta_1, \delta_2, \ldots\ ]^T$ are vectors of positive scalar design parameters, and where $d\{\delta\}$ and $d\{\alpha\}$ are the diagonal matrices defined by δ and α. Denoting the weighted error $\xi = d\{\alpha\}\triangle\mathbf{a}$, the structure

(20) and the hypothesis that, indeed, (8) is structurally valid lead to the estimation error dynamics

$$\frac{d}{dt}\xi = -d\{\delta\}\,\xi \;+\; d\{\alpha\}F(\mathbf{a})\triangle\sigma \tag{21a}$$

$$\frac{d}{dt}\triangle\sigma = -F\{\mathbf{a}\}^T\, d\{\alpha\}\,\xi, \tag{21b}$$

Under this *negative semi-definite + skew-symmetric* system structure, the storage (Lyapunov) function $V(\xi,\,\triangle\sigma) = 0.5(\|\xi\|^2 + \|\triangle\sigma\|^2)$ is non-increasing:

$$\frac{d}{dt}V(\xi,\,\triangle\sigma) = -\xi^T d\{\delta\}\,\xi \tag{22}$$

The stability implications of (22) imply heavily on invariance properties of (21), and, in turn, on the richness of the underlying trajectory of $\mathbf{a}$ (technically, on having *sufficient excitation*) (see, e.g., Artstein[21] and Anderson et al.[18]). With ample excitation error will decay and $\triangle\sigma \;\mapsto\; 0$. Design parameter selection effect the balance between dissipation rates and "error energy" flow, which need to be balanced for overall convergence.

B. Least Mean Squares Estimation

Here the curve fitting idea is followed literally. In the simplest form, the differential equation (8) is approximated as a difference equation

$$\mathbf{a}(t+\triangle t) = \mathbf{a}(t) + \{F\,[\mathbf{a}(t)]\;\sigma + G\,[\mathbf{a}(t)]\}\;\triangle t \tag{23}$$

with a small $\triangle t$. This equation can be re-cast in the form

$$A\sigma = \zeta \tag{24}$$

where the vector ζ contains the terms that are independent of σ in (23), evaluated at times t_k, $k = 0, 1, \ldots, K$ and $A\sigma$ describes, in an obvious manner, the corresponding σ dependent terms. This is an over-determined equality formulation that lends itself to a standard least mean squares estimation (or weighted versions thereof)

$$\sigma = (A^T A)^{-1} A^T \zeta \tag{25}$$

The *sufficient excitation* condition manifests itself as the invertibility of $A^T A$. The advantage of this method is that a constant solution is guaranteed. Yet in case the very structure of the model is incorrect, the value of that solution would be doubtful.

C. Parameter Estimation in the Cylinder Wake Benchmark

The mismatch between the Galerkin projection and observed dynamics is clear from Fig. 8 and in the top left plot of Fig. 9. An efficient estimation process exploits a clear distinction between two regimes: The near growth rate, characterizing the central transient domain, and the flat area of the attractor. Specifically ratios $\rho_r = \sigma_r/\beta$ and $\rho_3 = \sigma_3/\alpha$ determine the Galerkin system attractor, while the growth / dissipation coefficients σ_r and σ_3, in and of themselves, have essentially no impact in that region. Additionally, the cylindrical frames allow to estimate the frequency coefficients separately: Equation (4) can thus be re-written as

$$\dot{r} = \beta(\rho_r - a_3)r \tag{26a}$$

$$\dot{a}_3 = \alpha(r^2 - \rho_3 a_3) \tag{26b}$$

$$\dot{\theta} = \omega + \gamma a_3 \tag{26c}$$

Using this partition, α and β — which have no effect on the attractor — are first fixed at their nominal values and ρ_r and ρ_3 are estimated, using an attractor portion of the reference. Using either estimation scheme, the result is that indeed, the attractor is precisely predicted (the dotted line, top left plot of Fig. 9), but the growth rate is not resolved. Having fixed the corrected values ρ_r and ρ_3, estimation of the growth rates α and β exploits the growth portion of the reference. Indeed, it is convenient to convert (26a-26b) to

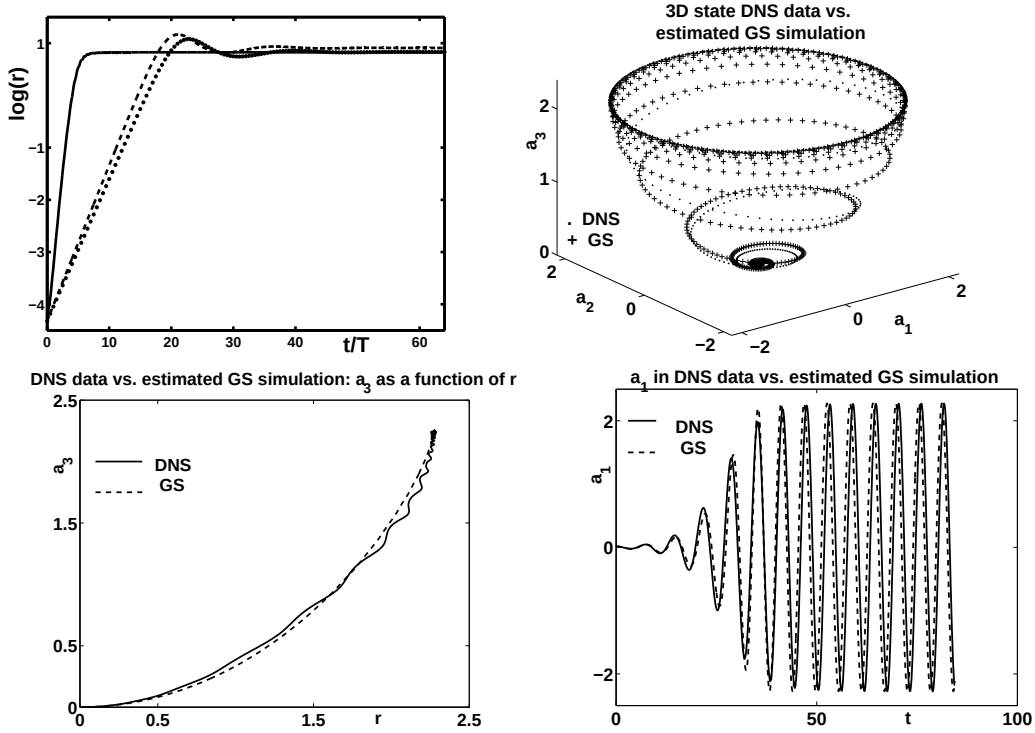

Figure 9. Top, left: The mismatch between $\log(r)$ growth in DNS (bold) and the the original Galerkin system response (dashed), where time is measured by T, the attractor's nominal period. Dynamic estimation of ρ_r and ρ_3 (from (26) with the nominal α and β) provide a match of the attractor (dots), but the growth rate is even lower than in the nominal model. The remaining 3 plots show the effect of estimating all model parameters, comparing Galerkin system and DNS simulations. Top, right: The 3D transient dynamics of the three leading Fourier coefficients. Bottom, left: a plot of a_3 as a function of r, along such transients. Bottom, right: The time trajectory of a_1.

Table 1. A comparison of nominal and estimated model parameters

Parameter	Nominal	Estimated	Estimated / Nominal
σ_r	0.048	0.1676	3.5
σ_3	0.048	1	20.8
β	0.019	0.0747	3.9
α	0.0196	0.4354	22.2
ω	-0.9936	-0.8524	0.86
γ	-0.034	-0.1091	3.2

equivalent differential equations in $\log r$ and $\log a_3$ to that end, using the near-linear portion of the transient reference. Again, these two estimation problems are mutually uncoupled. Finally, ω and γ are estimated from (26c). The results are plotted in the remaining three plots of Fig. 9, with near perfect tracking.
Table 1 compares the nominal and the estimated values of model parameters. To summarize the meaning of the differences between the nominal and the estimated model, we highlight the following points:

- *Differences in σ_r and β:* The factors of 3.5 / 3.9 indicate both a small correction to the amplitude of the resulting limit cycle, and a 3.5 fold increase in the initial exponential growth rate.
- *Differences in σ_3 and α:* The similar factors of 20.8 / 22.2 indicate that the target proportion of r^2 and a_3 is similar to the nominal prediction, yet the tracking speed is about 20 times faster.

- *Differences in* Ω *and* γ*:* The limit frequency is slightly lower. The 3.2 factor in γ was essential for good phase tracking during transients, and it reflects the deeper issue of phase shift in expansion modes during such transients.

Acknowledgments

The research of Gilead Tadmor was supported by the U.S. National Science Foundation grants ECS-0136404, CCR-0208791 and INT-0230489. Bernd R. Noack acknowledges support by the Deutsche Forschungsgemeinschaft (DFG) under grant NO 258/1-1, by the DFG via the Collaborative Research Center (Sfb 557) "Control of complex turbulent shear flows" at the Technical University of Berlin, by the DAAD program (PPP USA), and by the Windows of Science Program of EOARD. Stefan Siegel would like to acknowledge funding through the Air Force Office of Scientific Research, Lt.Col. Sharon Heise. We have profited from fruitful and stimulating discussions with the TU Berlin team (Ralf Becker, Oliver Lehmann, Rudibert King, Mark Pastoor, Ivanka Pelivan, Michael Schlegel, and Tino Weinkauf), with the US Air Force Team, (Kelly Cohen, Thom McLaughlin, and Mark Luchtenburg), and with Laurent Cordier (LEMTA).

References

[1]Noack, B.R., Tadmor, G., and Morzyński, M., "Low-dimensional models for feedback flow control. Part I: Empirical Galerkin models," *AIAA-Paper 2004-2408*, 2nd AIAA Flow Control Conference, Portland, Oregon, U.S.A.

[2]Unal, M. and Rockwell, D., "On the vortex formation from a cylinder; Part 1. The initial instability," *J. Fluid Mech.*, Vol. 190, 1987, pp. 491–512.

[3]Unal, M. and Rockwell, D., "On the vortex formation from a cylinder; Part2. Control by a splitter-plate interference," *J. Fluid Mech.*, Vol. 190, 1987, pp. 513–529.

[4]Mittal, S., "Effect of a "slip" splitter plate on vortex shedding from a cylinder," *Phys. Fluids*, Vol. 9, 2003, pp. 817–820.

[5]Strykowski, P. and Sreenivasan, K., "On the formation and suppression of vortex 'shedding' at low Reynolds numbers," *J. Fluid Mech.*, Vol. 218, 1990, pp. 71–107.

[6]Zhdanov, V. and Eckelmann, H., "The Effect of Jet Bleed on Base Pressure Distribution, Shedding Frequency, and Mean Velocity Profiles in the Wake Behind a Two-Dimensional Blunt Model," Tech. Rep. 9, Max-Planck-Institut für Strömungsforschung, 1990.

[7]Morzyński, M., Goujon-Durand, S., Noack, B.R., Wesfried, J., and Thiria, B., "Numerical analysis of the wake control behind a circular cylinder with oscillatory rotation," *Proceedings of XXI International Congress of Theoretical and Applied Mechanics 2004*, Warschau, Poland, August 15–21, 2004.

[8]Roussopoulos, K., "Feedback control of vortex shedding at low Reynolds numbers," *J. Fluid Mech.*, Vol. 248, 1993, pp. 267–296.

[9]Protas, B. and Styczek, A., "Optimal rotary control of the cylinder wake in the laminar regime," *Phys. Fluids*, Vol. 14, 2002, pp. 2073–2087.

[10]Hinze, M. and Kunisch, K., "Three control methods for time-dependent fluid flow," *Flow, Turbulence and Combustion*, Vol. 65, 2000, pp. 273–298.

[11]Bergmann, M., Cordier, L., and Brancher, J.-P., "Optimal rotary control of the cylinder wake using POD reduced order model," *AIAA-Paper 2004-2323*, 2nd AIAA Flow Control Conference, Portland, Oregon, U.S.A.

[12]Li, F. and Aubry, N., "Feedback control of a flow past a cylinder via transverse motion," *Phys. Fluids*, Vol. 15, 2003, pp. 2163–2176.

[13]Gerhard, J., Pastoor, M., King, R., Noack, B.R., Dillmann, A., Morzyński, M., and Tadmor, G., "Model-based control of vortex shedding using low-dimensional Galerkin models," *AIAA-Paper 2003-4262*, 33rd AIAA Fluids Conference and Exhibit, Orlando, Florida, U.S.A.

[14]Siegel, S., Cohen, K., and McLaughlin, T., "Feedback Control of a Circular Cylinder Wake in Experiment and Simulation," *AIAA-Paper 2003-3571*, 33rd AIAA Fluids Conference and Exhibit, Orlando, Florida, U.S.A.

[15]Noack, B.R., Afanasiev, K., Morzyński, M., Tadmor, G., and Thiele, F., "A hierarchy of low-dimensional models for the transient and post-transient cylinder wake," *J. Fluid Mech.*, Vol. 497, 2003, pp. 335–363.

[16]Noack, B.R., Tadmor, G., and Morzyński, M., "Actuation Models and Dissipative Control in Empirical Galerkin Models of Fluid Flows," *The 2004 American Control Conference*, Boston, MA, U.S.A., Paper **FrP15.6**.

[17]Ljung, L., "Black-box models from input-output measurements," *Proc. IEEE Instrumentation and Measurement Technology Conf., Budapest*, 2001, pp. 138–146.

[18]Anderson, B., Bitmead, R., Jr. C. J., Kokotović, P., Kosut, R., Mareels, I., Praly, L., and Riedle, B., *Stability of Adaptive Systems: Passivity and Averaging Analysis*, M.I.T. Press, Cambridge, MA, U.S.A., 1986.

[19]Lozano, R., Brogliato, B., Egeland, O., and Maschke, B., *Dissipative Systems Analysis and Control: Theory and Applications*, Springer-Verlag, Berlin, 2000.

[20]Ortega, R., Loria, A., Nicklasson, P., and Sira-Ramirez, H., *Passivity-based Control of Euler-Lagrange Systems*, Springer-Verlag, Berlin, 1998.

[21]Artstein, Z., "Stability, observability and invariance," *J. Differential Eqs.*, Vol. 44, 1982, pp. 224–248.